

Coronal Inflows and Giant Polar Plumes

R. Pinto^{*,†}, R. Grappin^{*} and J. L  orat^{*}

^{*}*Observatoire de Paris, LUTH, CNRS, 92195 Meudon, France*

[†]*Institut d'Astrophysique Spatiale, Universit   Paris XI, Orsay, France*

Abstract. We present the first results of simulations of giant polar plumes and coronal flows. We use a 2.5D axisymmetric MHD numerical model of an isothermal corona and slow solar wind. A plume is generated just above a small magnetic bipole embedded in an unipolar flux region which is perturbed by Alfv  n waves injected from the coronal base. The boundary conditions are transparent. The results are compared to those obtained previously with a 1D wind model in which plumes are generated as a consequence of variations of the heating and flux-tube expansion parameters.

Keywords: Sun, MHD, Polar plumes, Coronal jets, Solar wind

PACS: 96.60.-j, 96.60.P-, 96.60.pc, 96.60.Vg

INTRODUCTION

Polar plumes are jet-like overdense features seen over the polar regions, mostly during the low solar activity phases. These features extend radially, in the direction of the magnetic field in the coronal holes. Plumes are found to overlie EUV bright points, and these small bipoles appear to be undergoing interchange reconnection with the unipolar flux concentrations inside coronal holes. Outward propagating slow Alfv  n waves with periods between 10 and 15 min and amplitudes of about 10% – 20% of the plumes' intensity can be observed in the first $\sim 0.2 R_{\odot}$ [1]. [2, 3] studied the dissipation of such waves and its contribution to the coronal heating and solar wind acceleration. We focus here in the study of the formation and decay of coronal plumes (and associated in/outflows), and report some preliminary results of using an MHD numerical model of an isothermal axisymmetrical solar corona and wind. Alfv  n waves are meant to perturb a small magnetic bipole initially in steady-state equilibrium at the bottom of a unipolar coronal hole. The waves generate unsteady pressure patterns which lead to current density accumulation and reconnection. The results are compared to those found by [4] for a radially oriented magnetic flux tube which includes the dense chromospheric layers and the solar wind. In this later case, the wind is perturbed by rapid variations of the heating rate in the chromosphere and low corona, producing transient in and outflows before the system reaches a new steady-state equilibrium. Both cases show the formation of an overdense stream which progresses outwards in the form of a single wavefront with a phase velocity much higher than the bulk stream velocity (of the order of the surrounding wind speed). The decay of such features is accompanied by transient inflows visible mostly in the lower corona.

Photospheric forcing. Slow photospheric movements (null frequency) are expected to shear the coronal magnetic arcades by twisting their footpoints. This "twisting" may be transmitted upwards and so contribute to the magnetic tension/pressure accumulation, for as long as the magnetic diffusion remains negligible. Finite frequency movements, on the other hand, are more prone to inject waves (*e.g* sound and Alfv  n waves) into the very same magnetic structures. The standard numerical approach to the modelling of the effects of such movements is that of the rigid *line-tied* forcing of the magnetic loops by their footpoints, which are attached to the photosphere (both for the null and the finite frequency cases). An important consequence of this approximation is that total reflection occurs at the foot-points of the loops, which then act like resonant cavities; finite-frequency footpoint motions induce long-lasting and large amplitude oscillations [5] and null frequency motions shear the loop by an arbitrarily high amount. The *line-tying* approximation is, nevertheless, one among several possible approximations, and an extreme one in some senses. [6] have shown that, at least in the case of a single coronal loop perturbed by "slow" photospheric movements, the line-tying approximation may be inappropriate to characterise the coronal loop's dynamical response. In what follows, we will adopt an alternative approximation which diametrically opposes the *line-tying* one: we will consider an isothermal MHD corona with a *transparent* lower boundary (we'll name it the *fully transparent* case hereafter, for simplicity). We wish to stress at this point that both of these are extreme approximations, the physical reality laying somewhere in between. The *line-tied* case is prone to severely overestimate the energy input from the photosphere into the corona within magnetically connected regions, and the *fully transparent* case, on the other hand, underestimates it as the absence of the denser chromospheric (and photospheric) layers reduces the effective

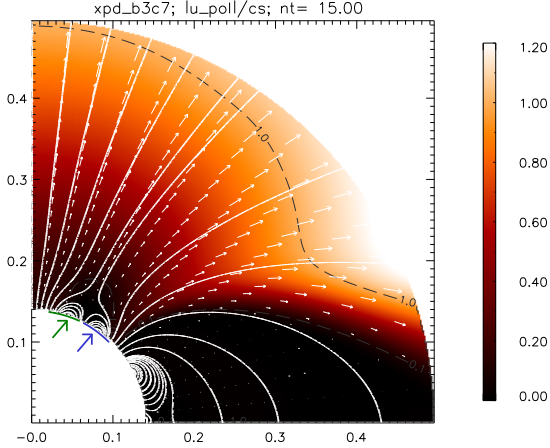


FIGURE 1. Initial conditions. Only the northern hemisphere is shown, and the radial sub-domain $1 \leq r/R_\odot \leq 3.5$. Color-scale represents the poloidal Mach number, the dashed contours levels $|u_{pol}|/c_s = 0.1, 1$. (with $c_s \approx 150$ km/s) and the white lines are magnetic field-lines. The large arrows show where Alfvén waves will be injected.

reflection ratios for waves crossing the lower regions. [7, 8] studied the wave energy leakage through these layers which, despite being non-negligible, may be smaller than other forms of energy dissipation. The rationale behind the present model (which uses the *fully transparent* approximation) is to consider a “pessimistic” configuration in what concerns the destabilisation of coronal structures and search for mechanisms which nonetheless are able to produce coronal events such as polar plumes, jets and inflows. More realistic (less extreme) situations will be considered in future work.

Heating. The ohmic dissipation and consequent heating will not be taken into account in our isothermal model, but the generation and accumulation of current density J can still be quantified. The analysis of the evolution of J in the domain may give clues to bridge and/or compare our results to others from non isothermal models.

GIANT POLAR PLUME

Numerical model. We use an 2.5 D axisymmetric model of the solar corona obeying the following one-fluid isothermal MHD equations

$$\begin{aligned} \partial_t \rho + \nabla \cdot \rho \mathbf{u} &= 0; \quad P = \frac{2}{m_H} \rho k_B T \\ \partial_t \mathbf{u} + (\mathbf{u} \cdot \nabla) \mathbf{u} &= -\frac{\nabla P}{\rho} + \frac{\mathbf{J} \times \mathbf{B}}{\mu_0 \rho} - \mathbf{g} + \nu \nabla^2 \mathbf{u} \\ \partial_t \mathbf{B} &= \nabla \times (\mathbf{u} \times \mathbf{B}) + \eta \nabla^2 \mathbf{B} \end{aligned}$$

The magnetic field \mathbf{B} decomposes into a time-independent *external* component \mathbf{B}^0 and an induced one \mathbf{b} . The solar wind develops into a stable transonic solution in the open field regions. Both the upper and the lower boundaries (respectively at $r = 14$ and $1.01 R_\odot$) are transparent. Alfvén waves are injected by perturbing the corresponding characteristic there. The diffusive terms are adapted so that grid scale (Δl) fluctuations are correctly damped. The kinematic viscosity is defined as $\nu = \nu_0 (\Delta l / \Delta l_0)^2$, typically with $\nu_0 = 2 \times 10^{14} \text{ cm}^2 \cdot \text{s}^{-1}$ and $0.01 \lesssim (\Delta l / \Delta l_0)^2 \lesssim 10$. The resistive term is replaced by an implicit filter which dissipates mostly at the grid scale and minimises the dissipation of large scales fluctuations. Note that actual kinetic dissipation should happen at scales much smaller than the grid size, so this approximation isn’t less realistic than a laplacian term. The principals of the numerical model are thoroughly discussed in [9]. The focus here is on circumventing the limitations found in [6] by means of a convenient choice of magnetic configuration (by setting \mathbf{B}^0) and Alfvén wave injection domain. In particular, we chose to perturb regions of the surface not directly connected by magnetic field lines, and we do so by starting from a magnetic configuration with a null point and separate connectivity domains. This way, we can expect wave mode coupling to happen due to the highly non-uniform phase velocity distributions, the existence of $C_s = C_a$ interfaces and very large Alfvén crossing times near the null point [10, 11].

Initial conditions. A close-up of the northern polar region of the numerical domain is displayed in Fig. 1. This particular configuration is comparable to the pseudo-streamer structures such as those in [12]. Monochromatic Alfvén waves will be injected in the zones indicated by the large arrows in Fig. 1. The wave period is in the range $T_0 = 6 - 35$ min, the amplitude $u_\phi^0 \approx 49$ km/s at the bottom of the corona and each side will be perturbed with a half period phase difference (such that pseudo-streamer structure oscillates as a whole). The plasma’s β is lower than 1 all along the lower boundary, and greater than 1 only over and around the null point.

Formation of a jet. The Alfvénic wave fronts produce a systematic (yet fluctuating) magnetic pressure gradient $\nabla b_\phi^2 / 2$ which push up the denser layers into the $\beta > 1$ region, force reconnection and plasma diffusion up into the open field region just above the null point. An over-dense plasma column forms continuously above the null point as the diffused plasma joins the solar wind. The jet presents a series of blobs, which correspond to density enhancements of amplitude $\frac{\delta \rho}{\rho} < 0.1$ which propagate upwards with a phase velocity equal to $u_{//} + c_s$ as slow mode wavefronts. (Fig. 2). The outermost edge of the jet progresses also with a velocity equal to $u_{//} + c_s$, above the jet’s bulk velocity $u_{//}$. The plasma

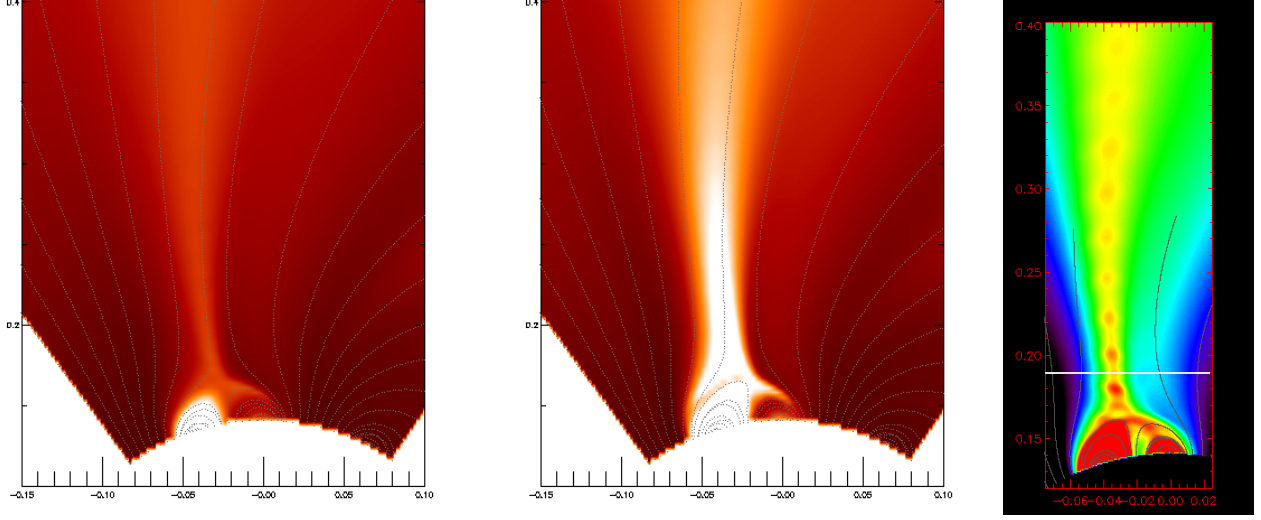


FIGURE 2. Formation of a jet above the bipolar structure in Fig. 1 (turned 30° CCW). The colour-scale represents ρ corrected to compensate for the stratification in the first $r \sim 3 R_\odot$ of the domain. The time intervals after the beginning of the wave injection are, from left to right, 2.5, 4.2, 5.9 and 7.5 h. The amplitude of the injected wave is $u_\phi^0 \approx 49$ km/s. The rightmost smaller image shows the instant $t = 7.5$ h with tighter colour ranges.

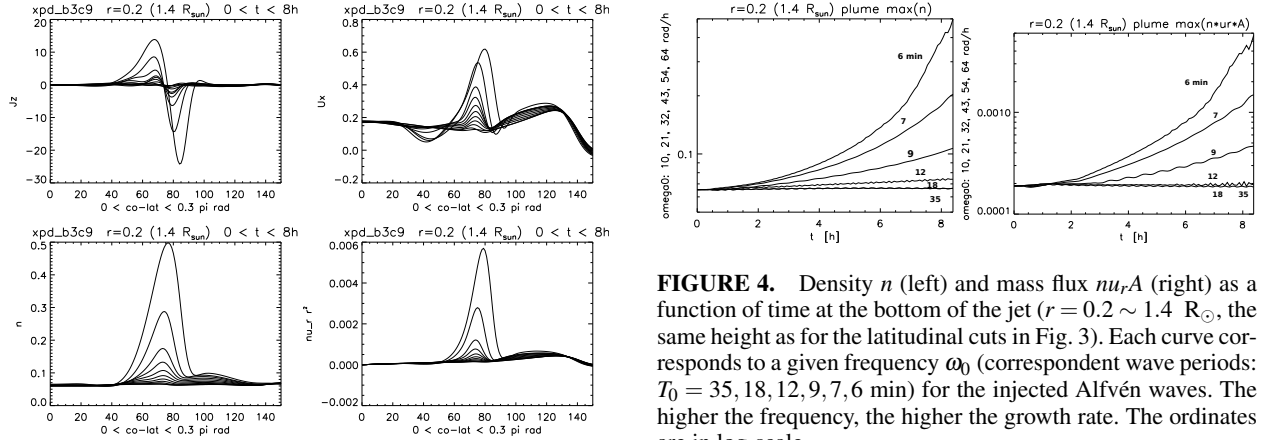


FIGURE 3. Profiles of J_ϕ , U_r , ρ , $\rho U_r r^2$ (top left, top right, bottom left and bottom right, respectively) over the white line in Fig. 2. Different curves correspond to different instants with $\delta t \sim 50$ min.

which does not join the jet falls back along both sides of the pseudo-streamer, producing two continuous inflows. Fig. 3 shows the evolution of the current density, radial velocity, density and mass flux over a cut represented as a white line in Fig. 2. A current sheet forms near the null point and along the magnetic separatrices as the plasma is compressed upwards. Current density peaks around the null point. The density contrast between the over-dense column and the background grows up to ~ 10 at the base of the jet but fades away at higher heights (~ 3 at $7 R_\odot$ and ~ 1 at $10 R_\odot$). The plasma's velocity becomes higher

than the surrounding solar wind within the jet, and so does the mass flux.

Growth rate vs. frequency. The Alfvén wave driven overdense jet may either saturate and reach a quasi-steady state or grow continuously for long periods of time, depending on the frequency ω_0 of the injected waves. Fig. 4 shows the growth of the mass flux and density within the jet as a function of time for several wave frequencies ω_0 . There is a smooth transition between a stable and an unstable regime at about $T_0 = \frac{2\pi}{\omega_0} = 12$ min; lower frequencies lead to lower (and eventually null) growth rates while higher frequencies lead to ever higher growth rates. This behaviour does not seem to break with time, at least for as long as the run lasts ($\Delta t \sim 8.5$ h).

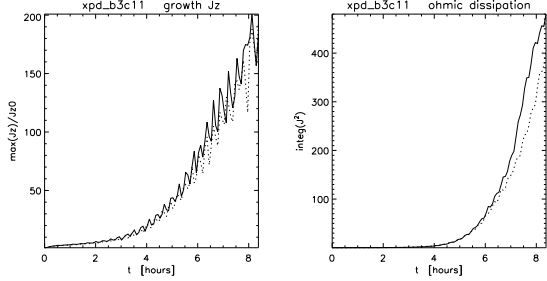


FIGURE 5. Left: peak current density $\max(J_\phi)/J_\phi^0$. Right: $\int_V J_\phi^2 dV$ in a volume V which encloses the perturbed region (magnetic bipole plus the lower part of the jet). The dotted line corresponds to a kinematic viscosity $2v_0$.

DISCUSSION AND CONCLUSIONS

We studied the long-term effects of finite frequency oscillations of the coronal footpoints of a pseudo-streamer placed inside a polar coronal hole using an MHD numerical model of an isothermal corona. We use transparent boundaries and show that perturbing such magnetic structures at their footpoints with Alfvén waves can lead to impressive large-scale phenomena. Transverse twisting movements at the base of the bipolar structure (Fig. 1) lead to a long lasting destabilisation of the system and the formation of a dense jet (Fig. 2) which may be interpreted as a polar plume. These movements are Alfvén waves injected at the base of the bipole, its two groups of magnetic arcades being perturbed in phase opposition one relative to the other. The effective twisting angle of the whole structure remains small (a few degrees) and oscillates with finite frequency, unlike in line-tied photospheric shearing models (e.g [13]). A complex pattern of Alfvén wavefronts propagating within the lower magnetic arcades non-linearly produces density enhancements which are pushed upwards, a part of which then diffuses across the magnetic field up into the open field region. The diffused plasma then joins the overlying polar plume. This diffusion shows a temporal modulation with a period equal to that of the injected waves (a consequence of exciting both magnetic arcades with exactly a half period phase difference; choosing different phase relations leads to different frequencies). As a result, the plume displays a series of blobs which propagate along its axis as slow mode wavefronts. This result is consistent with the slow waves observed by [1]. Current accumulates around the null point and along the magnetic separatrices. Fig. 5 highlights the growth of current density J_ϕ as a function of time and provides a measure of the production of magnetic small scales. The ohmic heating could be defined as $Q_{ohm}(t) = \eta \int_V J^2 dV$, where V encloses the perturbed region [14]. Note that the actual values of Q_{ohm} depend on the resistive settings and there-

fore on the local grid-scale, such that $Q_{ohm} \propto \Delta l^{-1}$. Varying the kinematic viscosity, on the other hand, has little effect on the result. Future work will bring deeper insight over the dissipative phenomena. The ohmic heating cannot be taken into account here (the model is isothermal), but we assume that the simulations of [4], who use a 1D non-isothermal model to study the dynamical effects of varying the heating rate and flux-tube expansion in the lower atmosphere, can represent an open flux tube passing close to the magnetic bipole in Fig. 1. The heating rate variations at low coronal heights are a proxy to the current accumulation and ohmic dissipation. Plume and interplume states are also obtained this way, with similar predictions for formation and decay time-scales and density contrast. On the other hand, the velocity of the wind for the plume solution they find is smaller than that for the interplume solution. To clear this point, we are working on extending the thermal treatment to the 2D case to have a unified (and self-consistent) view of these aspects.

ACKNOWLEDGMENTS

We thank the referee for useful suggestions. The numerical simulations were carried out using the IDRIS computing facilities.

REFERENCES

1. C. E. Deforest, and J. B. Gurman, *Astrophysical Journal* **501**, L217 (1998).
2. L. Ofman, V. M. Nakariakov, and C. E. Deforest, *Astrophysical Journal* **514**, 441–447 (1999).
3. L. Ofman, V. M. Nakariakov, and N. Sehgal, *Astrophysical Journal* **533**, 1071–1083 (2000).
4. R. Pinto, R. Grappin, Y. Wang, and J. Léorat, *Astronomy and Astrophysics* **497**, 537–543 (2009).
5. D. Berghmans, and P. de Bruyne, *Astrophysical Journal* **453**, 495 (1995).
6. R. Grappin, G. Aulanier, and R. Pinto, *Astronomy and Astrophysics* **490**, 353–356 (2008).
7. M. Gruszecki, K. Murawski, S. K. Solanki, and L. Ofman, *Astronomy and Astrophysics* **469**, 1117–1121 (2007).
8. M. Gruszecki, K. Murawski, and J. A. McLaughlin, *Astronomy and Astrophysics* **489**, 413–418 (2008).
9. R. Grappin, J. Léorat, and A. Buttighoffer, *Astronomy and Astrophysics* **362**, 342–358 (2000).
10. J. A. McLaughlin, and A. W. Hood, *Astronomy and Astrophysics* **459**, 641–649 (2006).
11. S. Landi, M. Velli, and G. Einaudi, *Astrophysical Journal* **624**, 392–401 (2005).
12. Y. Wang, J. B. Bierstecker, N. R. Sheeley, S. Koutchmy, J. Mouette, and M. Druckmüller, *Astrophysical Journal* **660**, 882–892 (2007).
13. E. Pariat, S. K. Antiochos, and C. R. DeVore, *Astrophysical Journal* **691**, 61–74 (2009).
14. L. Ofman, and J. M. Davila, *Astrophysical Journal* **476**, 357 (1997).